

# Fast Shared-Memory Barrier Synchronization for a 1024-Cores RISC-V Many-Core Cluster

Marco Bertuletti<sup>1</sup>[0000-0001-7576-0803], Samuel Riedel<sup>1</sup>[0000-0002-5772-6377],  
Yichao Zhang<sup>1</sup>[0009-0008-7508-599X], Alessandro  
Vanelli-Coralli<sup>1,2</sup>[0000-0002-4475-5718], and Luca Benini<sup>1,2</sup>[0000-0001-8068-3806]

<sup>1</sup> ETH Zürich, Rämistrasse 101, 8092 Zürich, Switzerland  
{mbertuletti,sriedel,yiczhang,avanelli,lbenini}@iis.ee.ethz.ch  
<sup>2</sup> Università di Bologna, via Zamboni 33, 40126 Bologna, Italy

**Abstract.** Synchronization is likely the most critical performance killer in shared-memory parallel programs. With the rise of multi-core and many-core processors, the relative impact on performance and energy overhead of synchronization is bound to grow. This paper focuses on barrier synchronization for *TeraPool*, a cluster of 1024 RISC-V processors with non-uniform memory access to a tightly coupled 4MB shared L1 data memory. We compare the synchronization strategies available in other multi-core and many-core clusters to identify the optimal native barrier kernel for *TeraPool*. We benchmark a set of optimized barrier implementations and evaluate their performance in the framework of the widespread fork-join Open-MP style programming model. We test parallel kernels from the signal-processing and telecommunications domain, achieving less than 10% synchronization overhead over the total runtime for problems that fit *TeraPool*’s L1 memory. By fine-tuning our tree barriers, we achieve  $1.6\times$  speed-up with respect to a naive central counter barrier and just 6.2% overhead on a typical 5G application, including a challenging multistage synchronization kernel. To our knowledge, this is the first work where shared-memory barriers are used for the synchronization of a thousand processing elements tightly coupled to shared data memory.

**Keywords:** Many-Core · RISC-V · Synchronization · 5G.

## 1 Introduction

With the slow-down of Moore’s Law at the turning of the century, multi-core systems became widespread, to sustain performance increase at an acceptable power budget in a scenario of diminishing returns for technology scaling [16]. Nowadays, the popularity of many-core systems increases, as they offer huge parallel computing power to achieve top performance on embarrassingly parallel workloads, from genomics over computational photography and machine learning to telecommunications [11, 14, 17]. For example, NVIDIA’s *H100 Tensor Core* graphic processing unit (GPU) features 144 streaming multiprocessors (SMs)

with 128 processing elements (PEs) [3], artificial intelligence (AI) accelerators such as *TsunAIMi* assemble 4 *RunAI200* chiplets [1] with 250 000 PEs within standard SRAM arrays for an at-memory design, *Esperanto's ET-Soc-1* chip has over a thousand RISC-V processors on a single chip and more than 160 MB of on-chip SRAM [5].

As the number of cores increases, scaling up architectures by instantiating many loosely-coupled clusters is a common architectural pattern adopted by many-cores to ensure modularity. However, this approach introduces overheads, including workload distribution, data allocation and splitting, inter-cluster communication and synchronization. To reduce these costs, increasing the cluster size is therefore desirable, as a direction space exploration the physical viability of this direction was demonstrated by *MemPool* [4, 15], which couples 256 RISC-V Snitch [19] PEs to a shared data memory ensuring low access latency. In this paper we further scale-up *MemPool* and increase the core count to 1024.

*MemPool* and *TeraPool* have a fork-join (the abstraction at the base of OpenMP) programming model: sequential execution forks to a parallel section, where PEs access concurrently the shared memory. Barriers are used to synchronize and switch back to the sequential execution. The cost of barrier synchronization is a relevant factor to determine the performance of a parallel program and scales with the number of PEs involved [12]. Despite the high core count, the synchronization overhead in *TeraPool* must be minimal, as we desire speedup also for kernels that do not have lots of work in each parallel thread. Moreover, synchronizing only some cores in the cluster must be possible, to ease workload distribution, increase the PEs utilization, and ensure more degrees of freedom in the parallel decomposition of a full application.

In this paper, we challenge the fork-join programming model, implementing fast barriers for a shared-memory tightly coupled cluster of 1024 cores. Our contributions include:

- A comparison of the synchronization strategies adopted on other large-scale many-core systems, with a focus on how the hierarchy of the hardware architecture affects the barrier implementation.
- The implementation of a central counter barrier and a k-ary tree synchronization barrier for *TeraPool*, exploiting hardware support to trigger the wakeup of all the PEs in the cluster or a fraction of them.
- An in-depth analysis of the performance of *TeraPool* on shared-memory parallel kernels synchronized with the implemented barriers, showing that the granularity of synchronization can be tuned on the basis of the kernel characteristics and that the barrier selection is an important stage of the kernel optimization.

A key insight is that tree barriers give up to  $1.6\times$  speed-up with respect to centralized barriers and less than 6.2% impact of synchronization on the total runtime of a full application from the field of 5G communications. Focusing on a RISC-V-based open-source many-core system enables us to provide an in-depth analysis of the synergies between our barrier implementations and the underlying hardware architecture. This is a key advantage over proprietary

vendor-specific solutions, where an incomplete disclosure of architecture prevents effective hardware-software co-design.

## 2 Related work

In the following, we survey relevant contributions on the synchronization of tens to hundreds of PEs. Most of the implementations focused on cached-based systems, with PEs grouped in hierarchies and sharing only the last-level cache.

In [13], an extended butterfly barrier was designed for Intel Xeon Phi *Knight's Landing* processor, whose 72 PEs, each having a private L1 data cache, are grouped in 32 tiles, connected by a 2D all-to-all mesh interconnect. The synchronization occurs in multiple stages, whereby a pair of threads notify each other of their arrival via atomic read and writes to synchronization variables. The architecture enforces cache coherence and the synchronization variables must be aligned to the cache boundary to avoid false sharing. The results indicate that at high core count, in such a fragmented and tiled many-core system, the butterfly barrier ( $\sim 2500$  cycles) outperforms less hierarchical centralized barriers ( $\sim 6500$  cycles) where a single master thread is responsible for verifying the PEs' arrival. In [6], tree barriers are tested on different many-core architectures with up to 64 ARMv8 cores. Authors focus on tournament barriers with a tree structure that fit the hierarchical core-cache organization of the underlying architecture, achieving a synchronization overhead of 642.5, 618.2, and 356 kilo-cycles on the *ThunderX2*, the *Pythion 2000+*, and the *Kunpeng920* processors, respectively. In [18], four barriers (single-master linear barrier, tournament tree barrier, butterfly barrier, and all-to-all barrier) are tested on the model of a scalable architecture with  $N_{PE}$  simple PEs connected together with a highly scalable network on chip (NoC) interconnect. Barriers were tested on different network topologies for up to 128 PEs. In highly connected NoC topologies, such as the *Torus*, barriers have less than 400 cycles synchronization overhead, and the all-to-all barrier, where any PE can simultaneously send a message to other PEs, performs the best. In a *Mesh* NoC, synchronization overhead takes up to 10 000 cycles for the all-to-all barrier but is limited to less than 1000 cycles for the tree and the butterfly barriers, as tree barriers become optimal when interconnect resources are reduced. In [7], the low core count (only 8 to 16 cores) of the multicore architecture makes hardware support for quadratic-complexity PE to PE signaling feasible and highly energy efficient. For the barriers implemented, the average length of periods where PEs can work independently from each other with 10% overhead of barriers corresponds to just 42 cycles.

In the context of GPU programming, the compute unified device architecture (CUDA) application programmable interface (API) has primitives that enable cooperative parallelism, including producer-consumer parallelism and synchronization across a thread group, the entire thread grid or even multiple GPUs [8]. From the hardware viewpoint, NVIDIA *Ampere* first added asynchronous barriers, with a non-blocking arrival phase that allows threads to keep working on independent data while waiting. When eventually all threads need data pro-

duced by others, they wait until everyone arrives, spinning on a shared variable. In *Hopper* GPUs, threads sleep instead of spinning while waiting, and transaction barriers are introduced to enable asynchronous copies of data [3]. Due to the proprietary nature of these tools, the behavior in hardware and the software implementation of GPU barriers is not entirely transparent.

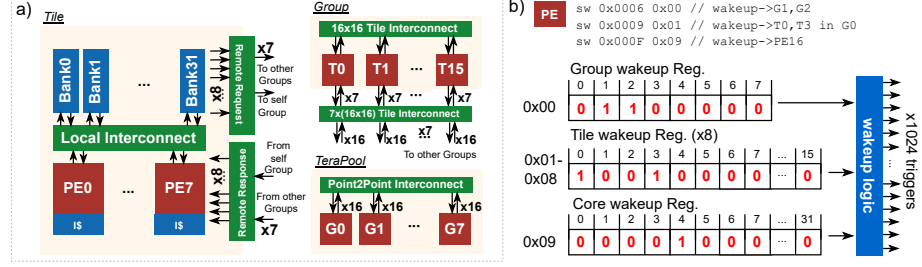


**Fig. 1.** a) The architecture of the *TeraPool* cluster and b) scheme of the implemented wakeup cluster registers and triggers.

*TeraPool* is the scaled-up version of the *MemPool* cluster presented in [4, 15]. The *TeraPool* cluster, represented in Fig. 1, has 1024 PEs tightly coupled to a multi-banked shared data memory. The access latency to any memory location is limited to 5 cycles, thanks to a hierarchical partition of the PEs and of the AXI interconnection resources. 8 PEs are grouped in a *Tile*, with single-cycle access latency to 32 local banks via a local interconnect. 16 Tiles are part of a *Group*. Each PE in a *Tile* can access the memory banks of another *Tile* in the same *Group* in less than 3 cycles, thanks to the Group-level 16x16 interconnect. 8 Groups build a cluster, and each PE can access a bank of a *Tile* in another *Group* in less than 5 cycles, though point-to-point connections between Groups. In a *Tile*, PEs share the interconnection resources towards another *Tile* in the same *Group*, and in a *Group*, Tiles share the interconnection resources towards another *Group*. Contentions may arise when more than one memory request tries to access the same memory bank or the same shared interconnection resource, leading to one of them being stalled for one cycle. The cluster has a non uniform memory access (NUMA) interconnect, but the low access latency in the case of no contentions makes *TeraPool* a good approximation of the parallel random access machine (PRAM) model [10].

In [6, 13, 18] the best performance of a barrier algorithm over another is strongly dictated by the interconnection topologies and by the clustering of PEs in hierarchies. In *TeraPool*, synchronization variables in any bank of the shared memory can be accessed at an almost equivalent and low cost, allowing to choose the granularity of barrier synchronization on the basis of the workload characteristics rather than of the topology of the interconnection between PEs and of the hierarchical partition of the hardware.

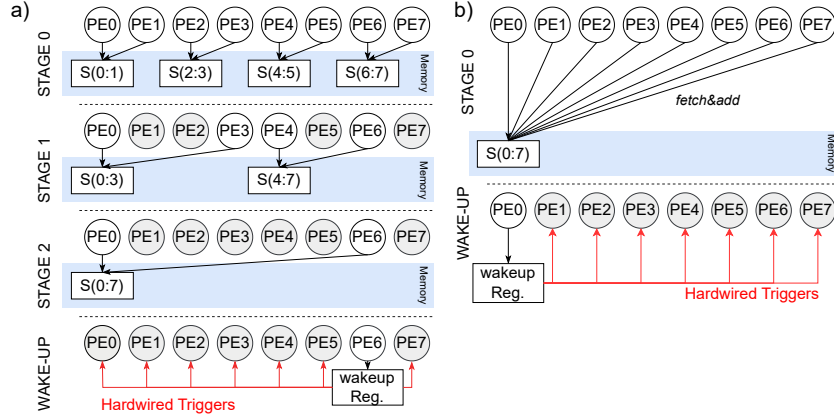


**Fig. 2.** a) Binary tree for the arrival phase of the barrier. Couples of PEs synchronize by atomically accessing shared synchronization variables. b) Central counter barrier.

### 3 Barriers implementation

In this section, we describe the implementation of our barrier primitives. A synchronization barrier algorithm can be divided into three phases: an arrival, a notification, and a re-initialization phase.

For the arrival phase, we adopt a  $k$ -ary tree. The  $N_{PE}$  cores of the cluster are divided into  $N_{PE}/k$  groups of  $k$  PEs. In each group, synchronization occurs in the form of a central-counter barrier [9]. Each PE arriving at the barrier updates a shared counter via an atomic *fetch&add* operation and goes into a wait for interrupt (WFI) sleeping state. The last PE reaching the synchronization step, fetches a counter value equal to  $k - 1$  and continues with the next steps, where it is further synchronized with the other  $N_{PE}/k - 1$  PEs that survived the first step. The last step counts  $k$  PEs, and the very last PE arriving wakes up all the PEs in the cluster. The arrival tree works best when the  $\log_k(N_{PE})$  is an integer, but it is also adapted to the case where  $k$  is any power of 2  $< N_{PE}$ , by synchronizing a number of PEs different from the radix of the tree in the first step of the barrier. Varying  $k$ , we encounter two extremes, represented in Fig. 2 (a-b): the left shows a radix-2 logarithmic tree barrier, where each step only synchronizes pairs of PEs, the right illustrates the central-counter barrier. The re-initialization phase is implemented concurrently with the arrival phase, as each PE arriving last in a synchronization step also resets the shared barrier counter before proceeding to the next step.

The notification phase leverages hardware support in the form of a centralized wakeup handling unit. The last PE arriving at the barrier and fetching from the shared barrier counter variable writes in a cluster shared register. The address of this register is in the cluster global address space and can be accessed by any core through the hierarchical AXI interconnections. The written value is detected by the wakeup handling logic that sends a wakeup signal to each individual

PE, triggering  $N_{PE}$  hardwired wakeup lines. A software implementation of the wakeup mechanism is excluded because it would fall into the single master barrier class [13], whose cost scales linearly with  $N_{PE}$  and is unsuitable for synchronizing more than a few tens of PEs.

We support synchronizing a subset of PEs in the cluster modifying the wakeup handling unit by adding other memory-addressable shared registers, as shown in Fig. 1. The core wakeup register is a 32-bit register that can be used to either trigger a wakeup signal to all the PEs in the cluster, when it is set to all ones, or to a single PE, by specifying its ID. One 8-bit register is used to selectively wake up Groups, and a register per Group is added to wake up Tiles in a Group selectively. A bitmask is used to determine the Groups or the Tiles to wake up. Depending on the bitmask written by a PE in one of the synchronization registers, the wakeup logic, asserts a subset of or all the wakeup triggers hardwired to the cores in the cluster, to trigger a wakeup signal.

The implemented barriers can be called from the function body through a custom software API. The radix of the barrier can be tuned through a single parameter, to ease trials and selection of the best synchronization option.

## 4 Benchmarking strategy

In the following, we describe the benchmarking strategy adopted to evaluate the performance of our barriers. Software is compiled with GCC 7.1.1 and runs on the open-source register transfer level (RTL) model of *TeraPool*, via a QuestaSim 2021.2 cycle-accurate simulation. In all the cases we assume that the input data resides in the L1 memory of the cluster.

### 4.1 Benchmarking with random delay

We first test the implemented barriers on the synchronization of PEs with a synthetic kernel implementing a random execution time for the parallel threads. The PEs start the execution together and proceed in parallel through a synchronization-free time interval. At this point, before entering the barrier, the cores are delayed by a number of cycles drawn from a uniform distribution between zero and a maximum delay. We track the average time spent by the PEs in the barrier. Since the result is subjected to the randomness of the delay, we average it over multiple tests. We also compute the fraction of the cycles spent in a barrier over the total runtime, as a function of the initial parallel section of the program only, referred to as synchronization free region (SFR). The goal is to estimate the minimum SFR for a negligible overhead, which is important information for the programmer on the granularity of the workload allocation to PEs.

### 4.2 Benchmarking of kernels

We analyze the performance of the barriers on benchmark kernels with a key role in the field of signal processing and telecommunications. The kernels are

implemented using a fork-join programming model, in which each PE operates on separate portions of the input data and accesses memory concurrently with the others. The final synchronization is achieved through a barrier call after all PEs completed their tasks. We can identify three classes of kernels:

- The *dot-product* (DOTP) and the *ax plus y* (AXPY) are implemented enforcing local access of the PEs to memory so that all the inputs can be fetched with one cycle latency. The data to be processed is equally divided between the PEs. The dot-product implies a reduction, which is implemented via the atomic addition of each PE's partial sum to a shared variable.
- In the *direct cosine transform* (DCT) and *matrix-matrix multiplication* (MATMUL) the workload is equally distributed between PEs, but we cannot enforce local access for all the PEs. Therefore, we expect some memory requests to take on average more cycles because of the inherent interconnection topology and contentions arising from concurrent parallel accesses.
- In the *2D-convolution* (Conv2D), the workload is not equally distributed because some PEs are just used to compute the image border, but the access pattern is locally constrained as seen for AXPY and DOTP.

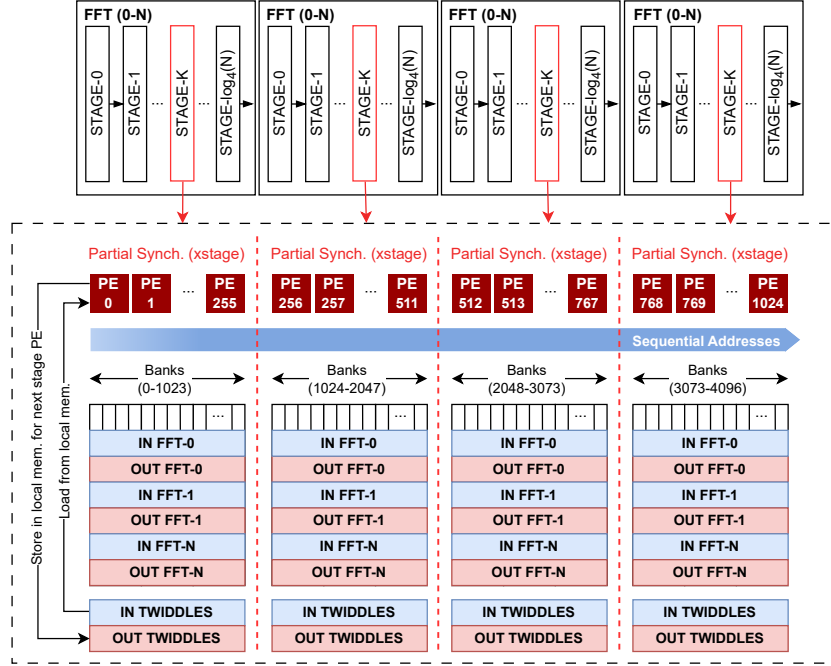


**Fig. 3.** Scheduling of  $N \times 4$  FFTs on *TeraPool*. Stage by stage, a group of  $N$  independent FFTs is scheduled on the same subset of PE, which are then partially synchronized.



### 4.3 Benchmarking of a 5G-processing application

Finally, we consider the implementation and performance of a full 5G application running on *TeraPool*, evaluating the impact of synchronization overhead on parallelization. We benchmark the Orthogonal Frequency Division Multiplexing (OFDM) demodulation stage of the lower Physical Layer (PHY) in 5G Physical Uplink Shared Channel (PUSCH), followed by a digital beamforming stage. In this workload,  $N_{RX}$  independent antenna streams, consisting of  $N_{SC}$  orthogonal sub-carrier samples, undergo a *fast Fourier transform* (FFT). The beamforming process is a linear combination of the antennas' streams, by known coefficients, producing  $N_B$  streams of  $N_{SC}$  samples. Between the two steps, there is a strong data dependency, and synchronization is needed.

The implemented radix-4 decimation in frequency FFT is a challenging multi-stage synchronization kernel, because PEs need to be synchronized after each butterfly stage. In a butterfly stage, each PE combines 4 inputs to produce 4 outputs. We can store the inputs locally in the same bank on different rows. Given the banking factor of 4, each core can work with the minimum access latency on  $4 \times 4$  input data and store the data in the local banks of PEs that will use them in the next FFT stage. A 4096-points FFT is therefore stored in the local memory of 256 PEs and processed by them, as shown in Fig. 3. Synchronization overhead is kept to the bare minimum: every FFT stage is run in parallel over a subset of PEs of the cluster. Cores working on different FFTs are independently synchronized, leveraging the partial barriers. Since a barrier is needed after each FFT computation stage, the PEs can load twiddles and work on multiple independent FFTs before joining, thus reducing the fraction of synchronization overhead over the total runtime.

Beamforming is implemented as a MATMUL between the  $N_B \times N_{RX}$  matrix of beamforming coefficients and the output FFT streams. Each PE computes a different output element, as the dot-product between a row and a column of the first and second input matrix respectively. The workload is distributed column-wise between 1024 PEs, so that each column goes to a different PE, while accesses to rows can happen concurrently.

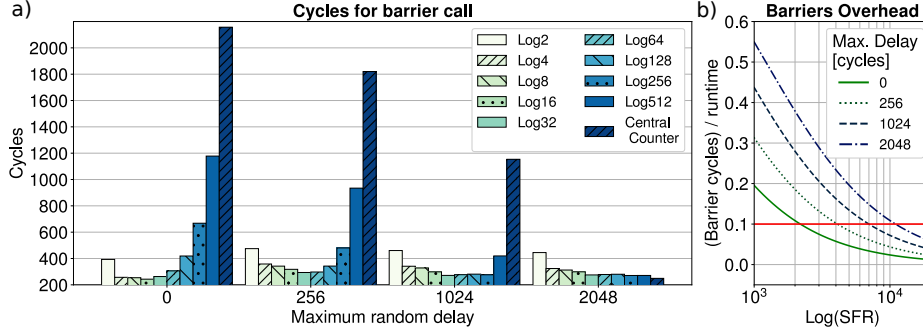
We try different configurations, as proposed in the 3rd Generation Partnership Project (3GPP) technical specifications [2]. Assuming  $N_{SC} = 4096$ , we consider a Multiple-Input Multiple-Output (MIMO) systems with  $N_{RX} = 16$ , 32 or 64 antennas and  $N_B = 32$  beams.

## 5 Results

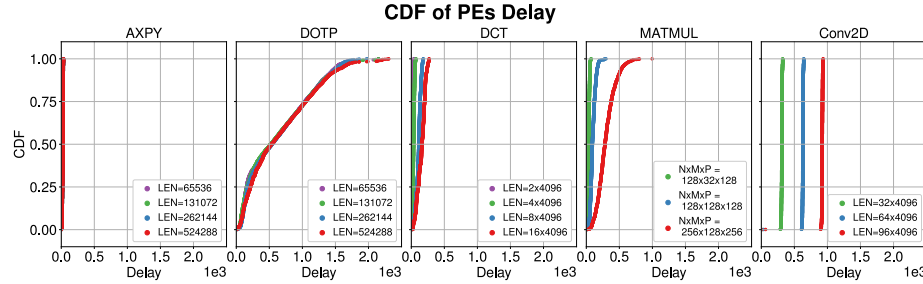
This section discusses the results of our benchmarking experiments. Fig. 4 (a) represents the cycles between the last PE entering and the last one leaving the barrier when each PE has a different random delay, extracted from a uniform distribution between zero and a maximum value. When the delay is zero for all PEs, the cycles for the barrier call exhibit a scoop behavior depending on the radix used. Low radix barriers require a longer multi-step synchronization



process. In this sense, the binary-tree logarithmic barrier is the worst, having 10 steps where PEs are synchronized in pairs. Barriers with few centralized synchronization variables require simultaneous access to the same memory locations by multiple PEs, creating banking conflicts. On this side, the linear central-counter barrier, where 1024 PEs conflict for the same memory location, is the worst. As the maximum delay increases, the PEs' arrival at the barrier is scattered. Therefore, contentions in accessing the synchronization variables reduce, and the lower radix barriers start to be more expensive than the higher radix ones, generating a staircase pattern. Ultimately, for the 2048 cycles delay, the central-counter barrier is the best, because cores requests to the barrier variable are sufficiently scattered in time to avoid contentions. The time that the last PE arriving at the barrier needs to traverse all the levels of the k-ary tree is, in this case, the most relevant part of the barrier runtime.



**Fig. 4.** a) Cycles between the last PE entering and leaving the barrier for different barrier radices, and maximum delays between the incoming PEs. b) Fraction of the best-performing barriers' overhead as a function of the SFR.



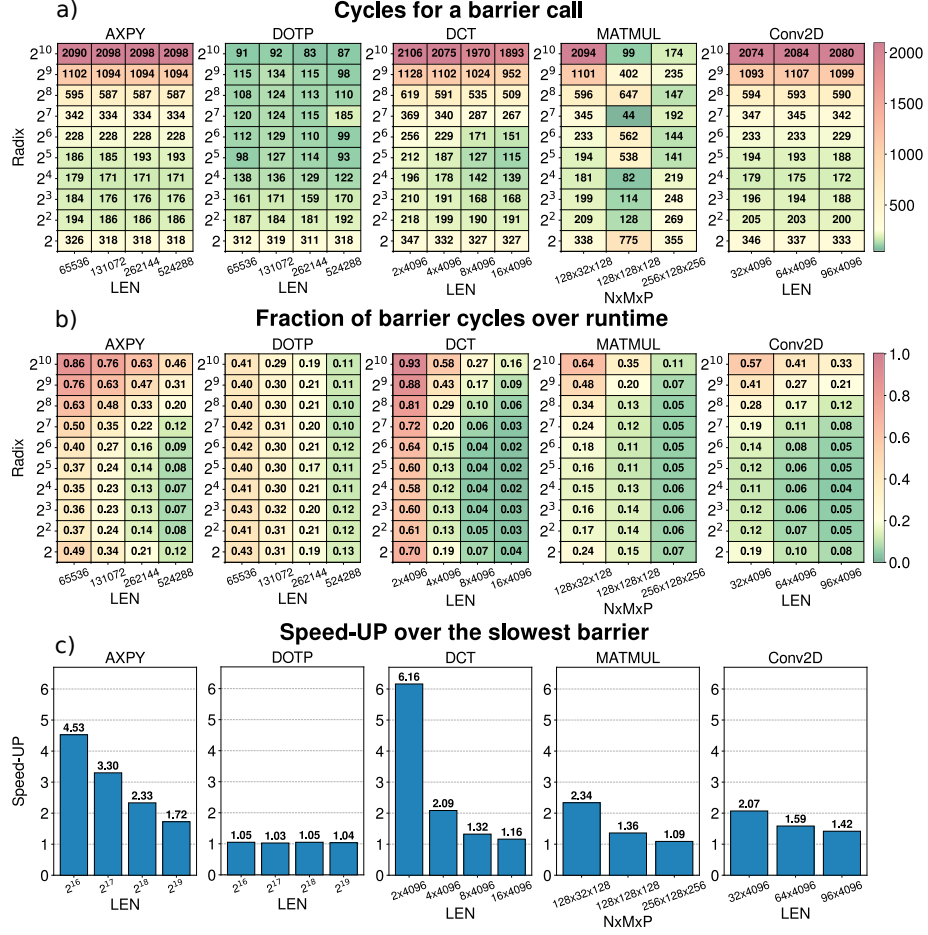
**Fig. 5.** CDF of the distributions of the difference between the fastest and the slowest PE runtimes for different exemplary parallel kernels before synchronization.

Fig. 4 (b) shows the fraction of the average cycles spent in a barrier by a PE, over the total runtime cycles, as a function of the SFR. The PEs' arrival is scattered as in the previous experiment. We consider different values of the maximum random delay between the PEs, and for each case, we report the results on the barrier with the best-performing radix. To achieve a synchronization overhead of less than 10%, our barriers need a SFR between 2000 and 10 000 cycles, depending on the scattering of the arriving PEs.

Since the arrival time of PEs is not always uniformly distributed, we measured the actual distribution for various key kernels and evaluated its impact on synchronization. Fig. 5 represents the cumulative distribution function (CDF) of the difference between the runtime cycles of the fastest and the slowest PE before synchronization for different parallel kernels.

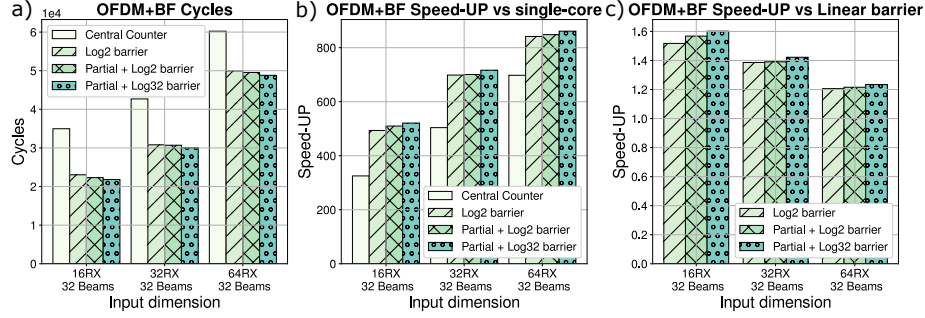
- The local access enforced for the AXPY and the DOTP kernels makes them conclude their job at the same time, independently of the input dimension. Contentions in accessing the reduction variable make some PEs slower than others for the execution of the DOTP.
- The access latency and the contentions in fetching memory locations that are distributed over the banks make the arrival of the PEs executing DCT, MATMUL, and Conv2D more scattered. The difference between the arrival time of PEs depends on the input dimension, because the larger the input data, the more the contentions. Interestingly the most compact distribution in arrival times for the DCT kernel is obtained for an input of length  $2 \times 4096$ . In this case, each PE works on two inputs of  $2 \times 2$  samples. Since *TeraPool* has 1024 PEs and a banking factor of 4, and the addresses run sequentially, the data is always stored locally.
- In the case of the Conv2D, we see a wide gap between the first and the last PEs arriving, which is caused by work imbalance. Some PEs are indeed assigned to the calculation of the boundary of the input image, which containing zeros is resolved in a lower number of instructions with respect to the pixels in the center of the image.

Fig. 6 (a) reports the delay between the last PE leaving the barrier and the last PE entering the barrier for different exemplary kernels, input dimensions, and radices of the k-ary tree barrier. The AXPY and the DCT find their sweet spot around radices 32 and 16 because the scattering in the arrival of PEs is moderate and the use-case falls in the scoop region on the plot in Fig. 4 (a). The arrival of the PEs in the Conv2D kernel is split between the fast cores computing the border of the input image and the slow cores computing the inner pixels, which are predominant, resulting in similar behavior to AXPY and DCT. The arrival of the PEs working on the DOTP kernel is scattered because of the reduction process. In this case, the lower-radix barriers have the worst performance, and the central counter barrier shows the best performance. We identify a behavior that is close to the staircase pattern on the right-hand side of Fig. 4 (a). The sparsity in the arrival of PEs strongly depends on the input dimension for the MATMUL kernel. Therefore, we find a small delay behavior for the very steep distribution obtained in the case of the input  $128 \times 32 \times 128$



**Fig. 6.** Colormaps of a) the delay between the last PE leaving and the last PE entering the barrier, b) the fraction of cycles for a barrier call (average on all PEs) over the total runtime, for different kernels, input dimensions, and barrier radices. c) Speed-up of the kernel synchronized with the fastest barrier on the kernel using the slowest barrier for each input dimension.

and a large delay behavior for the smooth distribution obtained in the case of the input  $256 \times 128 \times 256$ . The intermediate dimension has an intermediate behavior with some outlier points, caused by a peculiar feature of our barrier implementation: the synchronization of subsets of PEs in the leaves nodes of the tree barriers is initially performed on PEs with a contiguous index, therefore, mostly between PEs in the same Tile or in the same Group. These PEs share the interconnection resources, which are under stress during the execution of the MATMUL, and have a delay between them that slows down the first phase of the tree synchronization.



**Fig. 7.** a) Execution cycles for the 5G OFDM and beamforming with different synchronization barriers. b) Speed-up with respect to serial execution on a Snitch core. c) Speed-up with respect to the baseline using the linear central-counter barrier.

Fig. 6 (b) shows the average over all the PEs of the ratio between the barrier cycles and the total runtime for the selected kernels. The AXPY has a hot loop with few operations per input. Therefore, the problem dimension to achieve  $\sim 10\%$  overhead of the barriers is large. The DOTP, the MATMUL, and the Conv2D having a higher ratio of computations per input and steep CDFs of the PEs' arrival times, benefit of our tree barriers from small data dimensions. The SFR of the DOTP is large due to the PE scattering produced by reduction. This also requires large input vectors to make the barrier overhead negligible.

Fig. 6 (c) reports the speed-up on the total runtime obtained synchronizing with the fastest barrier option for every input dimension and kernel, compared to the slowest. Speed-up decreases as the input dimension grows because the barrier fraction on the total runtime reduces. For the DOTP speed-up is limited, because, as clearly shown on the right-hand side of Fig. 4, the gap between barriers is small when cores arrive scattered at synchronization. For all the other kernels, even in the case of large inputs, when synchronization consists of less than 10% of the total runtime, we report speed-up between  $1.1\times$  and  $1.72\times$ . This analysis proves that choosing the barrier radix based on the parallel kernel characteristics provides significant advantages.

Finally, in Fig. 7 we compare the performance of the central counter barrier, the tree barriers, and the partial barriers on the 5G OFDM and beamforming workload. Overheads account for the multi-stage synchronization required by FFT and the synchronization enforced by data dependencies between FFT and MATMUL. Fig. 7 (a) shows the execution cycles of the 5G application under exam for different numbers of antenna streams, and Fig. 7 (b) reports the speed-ups with respect to a sequential execution on a single Snitch core. The radix-4 4096 points FFTs are scheduled on the cluster as described in Fig. 3. We notice that using tree barriers greatly reduces the runtime with respect to using a central counter barrier, improving the serial speed-up. Constraining memory access to local addresses avoids a scattered arrival of the cores due to contentions, which explains the benefit obtained from tree synchronization. Further improve-

ment can be obtained by fine-tuning the radix of the tree barrier through the provided API and by introducing partial synchronization. The speed-ups with respect to synchronization using a central-counter barrier are reported in Fig. 7 (b). The best result of  $1.6\times$  is obtained using a radix-32 barrier and synchronizing only groups of 256 PEs working on independent FFTs. The overall speed-up reduces as the number of independent FFTs run between barriers increases. The inefficiency of the central-counter barrier slowly fades away as synchronization becomes a negligible part of the runtime. On our best benchmark, corresponding to the run of  $4 \times 16$  FFTs of 4096 points and of a MATMUL between a  $32 \times 64$  and a  $64 \times 4096$  matrix, the synchronization overhead accounts for just 6.2% of the total runtime. In this last case, we observe a speed-up of  $1.2\times$ .

## 6 Conclusions

This work challenged the fork-join programming model by scaling it to the 1024 cores of the *TeraPool* architecture. To leverage *TeraPool*'s full parallel workforce for parallel workloads, we focused on optimizing a key synchronization primitive: the shared memory barrier. We developed and optimized different software implementations of these barriers and added hardware support for the partial synchronization of groups of PEs in the cluster. We then tested our synchronization primitives on kernels of paramount importance in the field of signal processing. The average of the cycles spent by cores in a barrier over the total runtime cycles for the AXPY, DOTP, DCT, MATMUL, and Conv2D kernels is respectively as low as 7%, 10%, 2%, 5%, and 4%. On the sequence of OFDM and beamforming, a full 5G processing workload, which includes a multi-stage synchronization kernel (FFT), logarithmic tree barriers and the use of partial synchronization outperform the central-counter synchronization with a  $1.6\times$  speed-up. Our scheduling policy allows reducing the fraction of synchronization cycles over the total cycles to less than 6.2%.

Our results demonstrate that despite its high core count, the *TeraPool* many-core cluster behaves as a good approximation of the PRAM model with low synchronization overhead. This result relies on a tuned selection of the barrier flavor for a given target kernel.

**Acknowledgements** This work was supported by Huawei Technologies Sweden AG.

## References

1. runAI200 The Most Efficient AI Compute Engine Available. <https://www.untether.ai/products1>, accessed: 03.31.2023
2. 3GPP: 5G; NR; Physical layer procedures for data (3GPP TS 38.214 version 17.5.0 Release 17). Technical Specification (TS) 38.214, 3rd Generation Partnership Project (3GPP) (03 2023), version 17.5.0

3. Andersch, M., Palmer, G., Krashinsky, R., Stam, N., Mehta, V., Brito, G., Ramaswamy, S.: NVIDIA Hopper Architecture In-Depth. <https://developer.nvidia.com/blog/nvidia-hopper-architecture-in-depth/> (mar 2022), accessed: 2023-03-31
4. Cavalcante, M., Riedel, S., Pullini, A., Benini, L.: MemPool: A Shared-L1 Memory Many-Core Cluster with a Low-Latency Interconnect. In: 2021 Design, Automation & Test in Europe Conference & Exhibition (DATE). pp. 701–706 (2021). <https://doi.org/10.23919/DATE51398.2021.9474087>
5. Ditzel, D., Espasa, R., Aymerich, N., Baum, A., Berg, T., Burr, J., Hao, E., Iyer, J., Izquierdo, M., Jayaratnam, S., Jones, D., Klingner, C., Kim, J., Lee, S., Lupon, M., Magklis, G., Maric, B., Nath, R., Neilly, M., Northcutt, D., Orner, B., Renau, J., Reves, G., Reves, X., Riordan, T., Sanchez, P., Samudrala, S., Sole, G., Tang, R., Thorn, T., Torres, F., Tortella, S., Yau, D.: Accelerating ML Recommendation with over a Thousand RISC-V/Tensor Processors on Esperanto’s ET-SoC-1 Chip. In: 2021 IEEE Hot Chips 33 Symposium (HCS). pp. 1–23 (2021). <https://doi.org/10.1109/HCS52781.2021.9566904>
6. Gao, W., Fang, J., Huang, C., Xu, C., Wang, Z.: Optimizing Barrier Synchronization on ARMv8 Many-Core Architectures. In: 2021 IEEE International Conference on Cluster Computing (CLUSTER). pp. 542–552 (2021). <https://doi.org/10.1109/Cluster48925.2021.00044>
7. Glaser, F., Tagliavini, G., Rossi, D., Haugou, G., Huang, Q., Benini, L.: Energy-Efficient Hardware-Accelerated Synchronization for Shared-L1-Memory Multiprocessor Clusters. *IEEE Transactions on Parallel and Distributed Systems* **32**(3), 633–648 (2021). <https://doi.org/10.1109/TPDS.2020.3028691>
8. Harris, M., Perelygin, K.: Cooperative Groups: Flexible CUDA Thread Programming. <https://developer.nvidia.com/blog/cooperative-groups/> (oct 2017), accessed: 03.31.2023
9. Hoefler, T., Mehlan, T., Mietke, F., Rehm, W.: A Survey of Barrier Algorithms for Coarse Grained Supercomputers. *Chemnitzer Informatik Berichte* (jan 2004)
10. JaJa, J.F.: PRAM (Parallel Random Access Machines), pp. 1608–1615. Springer US, Boston, MA (2011). [https://doi.org/10.1007/978-0-387-09766-4\\_23](https://doi.org/10.1007/978-0-387-09766-4_23)
11. Li, H., Homer, N.: A survey of sequence alignment algorithms for next-generation sequencing. *Brief. Bioinform.* **11**(5), 473–483 (may 2010). <https://doi.org/10.1093/BIB/BBQ015>
12. Mellor-Crummey, J.M., Scott, M.L.: Algorithms for Scalable Synchronization on Shared-Memory Multiprocessors. *ACM Trans. Comput. Syst.* **9**(1), 21–65 (feb 1991). <https://doi.org/10.1145/103727.103729>
13. Mohamed El Maarouf, A.K., Giraud, L., Guermouche, A., Guignon, T.: Combining reduction with synchronization barrier on multi-core processors. *Concurrency and Computation: Practice and Experience* **35**(1), e7402 (2023). <https://doi.org/10.1002/cpe.7402>
14. Muralidhar, R., Borovica-Gajic, R., Buyya, R.: Energy Efficient Computing Systems: Architectures, Abstractions and Modeling to Techniques and Standards. *ACM Comput. Surv.* **54**(11s), 1–37 (sep 2022). <https://doi.org/10.1145/3511094>
15. Riedel, S., Cavalcante, M., Andri, R., Benini, L.: MemPool: A Scalable Manycore Architecture with a Low-Latency Shared L1 Memory (2023). <https://doi.org/10.48550/arXiv.2303.17742>
16. Theis, T.N., Wong, H.P.: The End of Moore’s Law: A New Beginning for Information Technology. In: *Computing in Science Engineering*. vol. 19, pp. 41–50 (2017). <https://doi.org/10.1109/MCSE.2017.29>

17. Venkataramani, V., Kulkarni, A., Mitra, T., Peh, L.S.: SPECTRUM: A Software-Defined Predictable Many-Core Architecture for LTE/5G Baseband Processing. *ACM Trans. Embed. Comput. Syst.* **19**(5) (sep 2020). <https://doi.org/10.1145/3400032>
18. Villa, O., Palermo, G., Silvano, C.: Efficiency and Scalability of Barrier Synchronization on NoC Based Many-Core Architectures. In: *Proceedings of the 2008 International Conference on Compilers, Architectures and Synthesis for Embedded Systems*. p. 81–90. CASES '08, Association for Computing Machinery, New York, NY, USA (2008). <https://doi.org/10.1145/1450095.1450110>
19. Zaruba, F., Schuiki, F., Hoefler, T., Benini, L.: Snitch: A Tiny Pseudo Dual-Issue Processor for Area and Energy Efficient Execution of Floating-Point Intensive Workloads. *IEEE Transactions on Computers* **70**(11), 1845–1860 (2021). <https://doi.org/10.1109/TC.2020.3027900>